Comparison of techniques to localise U-bearing particles in environmental samples

Aurélie Diacre, Pascal Fichet, Paul Sardini, Jérôme Donnard, Anne-Laure Fauré, Olivier Marie, Katsumi Shozugawa, Michaël Susset, Mayumi Hori, Takizawa Tsutomu, et al.

Comparison of techniques to localise U-bearing particles in environmental samples

Aurélie D.*[1,2], Pascal F.[3], Paul S.[4], Jérôme D.[5], Anne-Laure F.[1], Olivier M.[1], Katsumi S.[6], Michaël S.[1], Mayumi H.[6], Takizawa T.[6], Fabien P.[1], Olivier E.[2]

[1]Commissariat à l'Energie Atomique et aux énergies alternatives (CEA, DAM, DIF, F-91297 Arpajon, France.

[2]Laboratoire des Sciences du Climat et de l'Environnement (LSCE/IPSL), Unité Mixte de Recherche 8212 (CEA/CNRS/UVSQ), Université Paris-Saclay, Gif-sur-Yvette, France.

[3]DES-Service d'Etudes Analytiques et de Réactivité des Surfaces (SEARS), CEA, Université Paris-Saclay, 91191, Gif-sur-Yvette, France.

[4]Université de Poitiers, UMR CNRS 7285 IC2MP / HYDRASA, rue Michel Brunet, 86022, Poitiers Cedex, France.

[5]Ai4r, 2 Rue Alfred Kastler, 44307 Nantes, France.

[6]The University of Tokyo, Graduate School of Arts and Sciences, Tokyo 153-8902, Japan.

Abstract

This publication shows results of a comparison of three techniques for localising radioactive, and U-bearing particles on same samples. Particles are localised by the means of three methods: (1) Fission Tracks (FT), (2) Imaging Plate (IP), and (3) real time autoradiography (BeaQuant®). These techniques were applied to various samples, including a sediment sampled in

the vicinity of the Fukushima Dai-Ichi Nuclear Power Plant (FDNPP) and a sample made of pure U oxide particles. In addition, the efficiency of the combination of two methods (FT and IP) to localise specifically anthropogenic U-bearing particles was tested.

Key words

BeaQuant®, imaging plate, fission tracks, alpha and beta emitters localisation, uranium.

1. Introduction

Nowadays there is a real need for the detection and characterisation of anthropogenic radioactive particles contained in soils/sediments to assess the exposure of human beings to ionizing radiation and its consequences on health and the environment. These particles have been emitted during nuclear accidents such as Chernobyl [1–3], Fukushima Dai-Ichi Nuclear Power Plant (FDNPP) [4–16], Thulé [17, 18], and Palomares [19–21] or have been released from nuclear facilities during nuclear fuel cycle operations [22]. Actinides are particularly interesting because of their long persistence in the environment (24.11×10^3 years for ^{239}Pu to 4.47×10^9 years for ^{238}U) and can therefore be used as a sediment tracer [23]. For accurate assessment of the environmental impact of these particles and associated risks, it is important to be free from other sources of actinides like natural uranium bearing minerals or global fallout from past nuclear weapon tests. Thus when performing traditional bulk analysis on soil or sediment samples, the resulting isotopic and elemental composition is a mixing of all these actinide sources. Only particle analysis that consists in the characterisation at the particle scale enables to focus on the emission source of interest.

The goal of this work is to investigate nuclear fuel-bearing particles and to study the detection capacities of three techniques: (1) the fission track method, based on the fissile properties of ^{235}U and ^{239}Pu, (2) real time α-autoradiography, based on the detection of α-emitting isotopes (^{234}U, ^{235}U, ^{238}U, ^{239}Pu, ^{240}Pu) and (3) α-autoradiography on imaging plates. Since the 1990's, the fission track method has been implemented for the detection of particles containing uranium and plutonium in safeguards samples [24] and is very sensitive to high enriched uranium bearing particles. In the field of medical biology and geosciences, a new real-time digital autoradiography method is already in use, the BeaQuant® (Ai4R, Nantes, France). This device, implemented on thin slides of rocks [25] and on biological samples, enables a quantitative chemical mapping of alpha emitters. The last method based on the use of imaging plates is commonly used in the literature to detect particles containing β-γ emitters [4–6, 8–16, 26, 27]. These β-γ emitters may be actinide decay products or fission products such as ^{137}Cs if nuclear fuel has been irradiated. In this paper, we implemented the imaging plate method developed by [27] to detect specifically α-emitters.

To our knowledge, these three detection-localisation techniques are compared for the first time for two different types of samples: (1) pure U oxide micro-particles (highly enriched U with a 40% atomic abundance of ^{235}U); and (2) a sediment sample collected in the vicinity of FDNPP with significant (> 10,000 $kBq \cdot kg^{-1}$) β and γ emitter activities that may contain nuclear fuel particles. Besides, a grass sample (IAEA 472 CRM) that contains only β and γ emitters was also prepared as a control sample. We also describe the different limitations of each method. Actually, the presence of naturally occurring nuclides such as uranium (α emitter) and its decay products (mainly β-γ emitters) in soils/sediments may hide the presence of anthropogenic particles specifically in case of volcanic U-rich soils for example. Moreover, in the case of irradiated nuclear

particles, radioactive emissions from actinides are mostly negligible compared to the proportion of β-γ emissions from fission products (^{137}Cs, etc.). The fission products may generate interferences on α-autoradiography detection. In addition to this comparison exercise, theoretical numbers of FT and α-tracks generated for the U-bearing particles from both samples (pure U and FDNPP U-bearing particles) were calculated assuming given transmission and auto-adsorption coefficients.

2. Material and methods

2.1. Sample collection and preparation

A sediment sample referred to as Okuma was collected at 2.7 km to the West of FDNPP, in Choja-bara, Otto-zawa, Okuma Town, Fukushima Prefecture, Japan (37.42230°N 141.00345°E) (**Fig. 1**) on March 18, 2014 within the Restricted Zone. The specific activity of ^{137}Cs was 13,300 kBq·kg^{-1} (± 18 kBq·kg^{-1}) at the time of analysis. About 1 g of the sample was dry-sieved to 63 µm. The sample fraction was then suspended in a mixture of ethanol and of an organic polymer (collodion) and spread on Lexan® disks (Lexan®, General Electric Plastic, USA). Coating with collodion was necessary both to immobilize particles and to prevent contamination of the detection media. Three disks referred to as 20B2, 20B16, and 20B20, were prepared and used for the experiments. A process blank was also prepared with the same method.

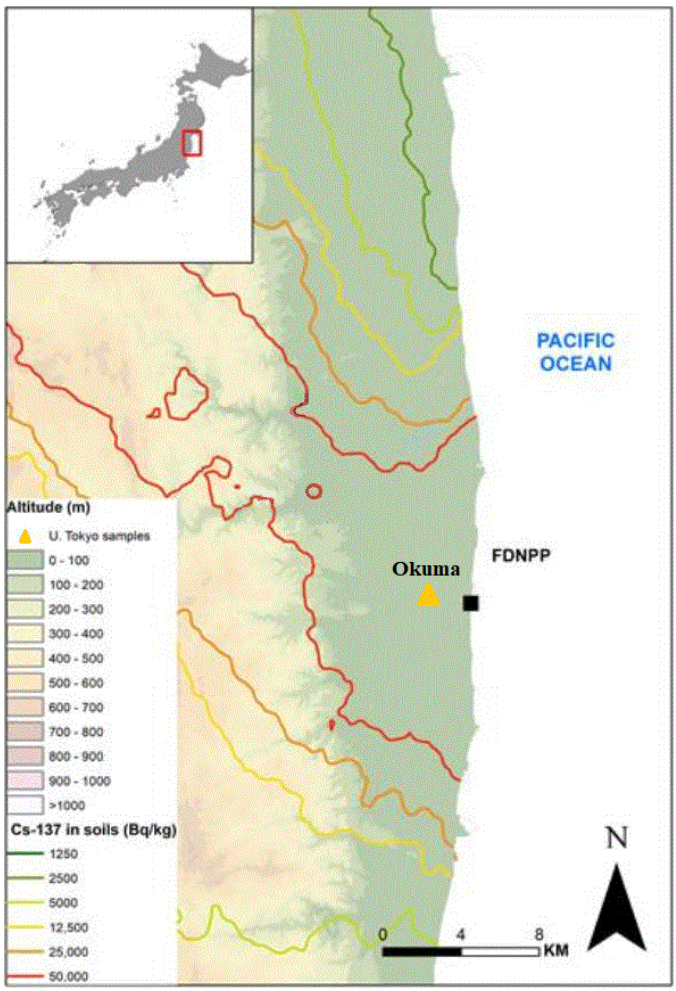

Fig. 1 Background ^{137}Cs level map in soils of the Fukushima prefecture after Chartin et al. (2013) with location of the Fukushima Dai-Ichi Nuclear Power Plant (FDNPP, black square) and the investigated sediment sample (yellow triangle).

Moreover, a subsample of the IAEA-472 certified material was also analysed as a control sample. This material, collected in Polesskoe, Kiev, Ukraine during summer in 1990, is a grass sample, which contains only β and γ emitters like ^{40}K and ^{137}Cs with a reference weight activity decay-corrected to 2020 of 1 kBq·kg^{-1} in ^{40}K and 8 kBq·kg^{-1} in ^{137}Cs. This standard sample was prepared using the same protocol as for the Okuma sample and dispersed onto two Lexan® disks

(1 mg, i.e. ≈ 4.1×10^{-3} Bq of ^{137}Cs per disk). The analysis of this certified material was used to estimate the contribution of β emissions during BeaQuant® acquisitions.

Finally, samples containing highly enriched uranium micro-particles (HEU MP) with a ^{235}U atomic abundance of 40 % referred to as 19A32 and 19A33 were also used as a reference for α-emitters because their specific α-activity (α-activity by mass unit) is higher than those of the naturally-occurring (non-purified) U (by a factor of ~6) and of the U from reactor 3 (without Pu) from FDNPP (by a factor of ~17). Therefore, we expect to have greater chances to detect such pure HEU particles by α-autoradiography techniques instead of natural mineral particles rich in U for the same U content. These particles, whose equivalent diameters range between 250 and 400 nm, were mixed with urban particulate matter (SRM 1648a, National Institute of Standards and Technology, USA) that contains element like aluminium, silicon and lead which are expected to be found in industrial environments. This SRM contains also natural U with an estimated concentration about 5 $mg \cdot kg^{-1,}$ which is slighlty larger than the estimate of the average concentration of U in soil (~ 3 $mg \cdot kg^{-1}$). The estimated mass of natural U was equal to about 16 ng and the mass of HEU equal to about 32 ng [29]. These particles were trapped in a piece of cotton and were extracted from the cotton tissue in an ultrasonic bath filled with ethanol. After mixing with the organic polymer, particles were deposited on Lexan® disks like the Okuma sample.

2.2. Methods for localising radioactive particles implemented in this study

2.2.1. Imaging Plates (IP) technique

The imaging plate (IP) is a passive, two-dimensional radiation detector based on the photo-stimulated luminescence (PSL) phenomenon [30, 31]. Due to their high sensitivity over a large

range of energy levels, IPs applications are widely used in medical and environmental sciences. There are three types of IPs: (1) TR (Tritium), (2) MS (Multipurpose Standard), and (3) SR (Super Resolution). Differences between these IP types are: (1) the absence of protective layers for the TR type and (2) variable thickness of the sensitive layer between IP types. In all of them, the active layer is made of a photo-stimulating phosphor crystal, typically $BaF(Br,I):Eu^{2+}$ [31]. When exposed to an ionizing radiation − energetic charged particles, X-rays, or γ rays − some of the incoming ionizing particles deposit a part of their energy which is stored in the phosphorous layer in the form of FBr^- or FI^- centres and Eu^{3+} ions [30]. The electrons that are trapped in these sites, can be later released by visible light irradiation and reintegrated into the Eu^{3+} ions followed by the emission of 3 eV photons called PhotoStimulated Light (PSL) [30]. The emitted light in the blue part of the visible spectrum can be detected, usually by means of a photomultiplier tube (PMT), and its intensity is proportional to the incident radiation intensity recorded in the IP [33] with a very large dynamic range of intensity, typically spanning five orders of magnitude.

To be used as a detector, IP must be calibrated for both the PSL response to radiation (energy and type) and for spatial resolution. The IP calibration is done with known activity sources and different exposure times [34]. In this study, we implemented TR films (IP, TR 12.5 cm × 25.2 cm, Perkin Elmer) without a protective layer to increase the probability of detecting α emissions at very low levels of activity from actinide-bearing particles. A methodology based on the overlay of several IPs to try to identify different radioisotopes was developed [27]. Indeed, γ rays and electrons can imprint several IPs depending on their energy while α particles can only impact the first (closest to the same sample) IP. Here, we applied this method by overlaying two IPs to discriminate the impact of β and γ versus α-particles. The IP in contact with prepared disks (IP1) allows recording α, β and γ PSL and the second IP (IP2) allows recording of only γ and β PSL.

Therefore, PSL emissions observed only for IP1 and not for IP2, or significantly stronger for IP1 than for IP2, are very likely to indicate that samples contain α-emitters.

Two disks of the Fukushima sample (Okuma) and two disks of the HEU MP were analysed with this device for an acquisition time of two weeks in the darkness in lead shielding (Supplementary information A). This acquisition time was set to improve the chance to detect alpha emission without much loss of sensitivity due to fading effect. Autoradiography images were then recorded using the IP reader (Cyclone Plus, Perkin Elmer) with a pixel size of 150 dpi (dot per inch) corresponding to one measurement each 169 µm in the IP screen. The IP reader quantified the radiation intensity as PSL for each pixel (a total of 749 × 1452 pixels) and stored it in a TIFF image format.

To identify high-radioactivity spots, the autoradiography images of IP1 (**Fig. 4a**) and IP2 (**Fig. 4b**) were processed using the ImageJ software (https://imagej.nih.gov/ij/) in order to report the PSL values of each IP pixel in a table. Raw PSL values were corrected by the software's drift values of the IP reader (Eq. (1)).

$$PSL_{\,Corrected\,IP1} = PSL^2 \times 2.34 \times 10^{-5} \quad (1)$$

For the IP2 the same calculation takes into account the loss factor of β-γ between the two IP, which determined to be 0.18 from a ^{137}Cs source [27] (Eq. (2)).

$$PSL_{\,Corrected\,IP2} = PSL^2 \times 2.34 \times 10^{-5} / 0.18 \quad (2)$$

To highlight hot spots corresponding to α emissions only, the PSL-corrected values of the IP2 were subtracted from the PSL-corrected values of the IP1 (Eq. (3)).

$$PSL_{1-2} = PSL_{\,Corrected\,IP1} - PSL_{\,Corrected\,IP2} \quad (3)$$

Finally, $PSL_{1\text{-}2}$ was corrected for the background and the standard deviation (Eq. (4))

$$PSL_{1-2} = PSL_{1-2} - mean_{background} - 3 \times RSD_{background} \quad (4)$$

Results of the processed IP PSL were then converted into a new autoradiography image with ImageJ to visualize hot spot locations (**Fig. 4c**).

2.2.2. Fission Tracks (FT) technique

An additional Lexan® disk, acting as solid state nuclear track detector and referred to as "FT disk", was welded onto each Lexan® disk onto which the particulate sample was deposited (referred to as "deposition" disk). The disks were then packed into a capsule and irradiated in the TRIGA nuclear reactor (Jozef Stefan Institute, Ljubljana, Slovenia). A specific irradiation device was used for that purpose in order to get a well-thermalized neutron flux with a high fluence, in the 10^{15} neutron cm^{-2} range, to be able to detect particles with low numbers of fissile nuclei [35]. Fissile nuclides (^{235}U, ^{239}Pu) underwent a fission reaction during which two fission fragments were emitted. These fragments then impacted the Lexan® disks and modified their surface structure [24]. After irradiation, the FT disk was chemically etched to make FT visible under an optical microscope. The sea urchin-shaped FT clusters are characteristic of the presence of a fissile nuclide-bearing particle. With appropriate landmarks on both deposition and revelation Lexan® disks, it is possible to locate the particle that produced the FT cluster.

FT clusters may come from either (1) a mineral particle of significant size with a sufficiently high content of naturally-occurring U (like zircons, monazite or granites), or (2) a particle coming from the FDNPP which contains human-modified U (i.e. purified and enriched in fissile ^{235}U isotope) and possibly ^{239}Pu (produced within the nuclear fuel by neutron capture or initially added to UO_2 to make a MOX fuel). Once the particle localised, its source can be identified by combining the determinations of the elemental composition from SEM-EDS and of the U isotopic composition by secondary ion mass spectrometry.

2.2.3. BeaQuant® technique

The BeaQuant® is a digital autoradiography real-time acquisition system based on the use of a gaseous detection medium [25, 36]. The micro-pattern gaseous detector (MPGD) incorporates a micromesh parallel ionization multiplier (PIM) [37–39]. In this gas mixture, charged particle emitted by the sample interact with the gas and release their energy by ionization of the gas mixture. Exposed to appropriate electric fields, the electrons created during the interaction are multiplied, drifted and sent to the segment anode. A α-disintegration triggering the electronic acquisition is thus reported on an autoradiography image in real time. BeaQuant® has the capability to count and map α or β-emitting particles without influence of γ emitters [25, 37] and with a high spatial resolution (maximum resolution of 20 µm for both α and β from tritium detection [39, 40]. With the MPGD, the BeaQuant's® sensitivity is about 5×10^{-5} cps·cm^{-2} for a U concentration of 2 ppm at secular equilibrium [25], with a detection linear response of 5 orders of magnitude [37]. Moreover, by adjusting the BeaQuant® amplification gains, it is possible to discriminate α and β emissions.

However, samples analysed with BeaQuant® need to be perfectly flat: any surface roughness can induce artefacts corresponding to artificial hot spots on the autoradiography image. The sample preparation carried out in this study is therefore perfectly appropriate for BeaQuant® analyses. Disks were placed during four days within a GS-1010 sample holder (10 cm × 10 cm), in front of the gas detector and analysed with the measurement parameters configured for ^{238}U in order to detect α emitters (referred to as method 1) specifically. As Fukushima samples are highly contaminated with ^{137}Cs (>10 kBq·kg^{-1}), a second acquisition was realized with a configuration more restrictive on U energy in order to avoid ^{137}Cs detection (referred to as method 2). The

acquisition time was set to ten days because the sensitivity was reduced with these settings. The IAEA-472 standard sample was also analysed by method 2 in order to check the decrease in background due to the energy limitation. For method 2, the pixel size chosen for the analysis reached up to 50 µm and increased to 400 µm after post-processing in order to integrate a stronger signal per pixel.

After acquisition with both methods, post-processing was conducted to remove the β contribution. Betas were identified by their significant contribution in the low amplitudes. The filtering consisted of removing these low amplitude signals to keep the background noise as low as possible.

2.3. Morphological and elemental characterisation of the particles by SEM-EDS (Scanning Electron Microscopy - Energy Dispersive Spectroscopy)

A scanning electron microscope (FEI Quanta^{TM} 3D FEG (Field Emission Gun), Eindhoven, The Netherlands) equipped with backscattered and secondary electron detectors was used to determine the size, the morphology and the elemental composition of the particles.

Elemental analyses on particles were realized in-situ via EDS with an Octane Elect Plus detector (EDAX, Ametek, Tilburg, The Netherlands), which has a surface area of 30 mm². Analyses were performed with an accelerating voltage of 30 kV to detect U X-ray at 13.6 keV.

3. Results and discussion

3.1. Theoretical performance of the three methods

Theoretical calculations were made to estimate the numbers of (1) α emissions and (2) FT depending on the elemental/isotopic composition and the size of the particle. In this section, we

considered a pure UO_2 particle with a density of 10.97 g·cm^{-3} and a ^{235}U abundance corresponding to that of fresh FDNPP fuel (^{235}U = 3.7 atomic %). We considered also spent FDNPP UO_2 fuel of reactor 3 containing 0.7 wt% of Pu [41], MOX fuel of the reactor 3 containing 0.05 g·g^{-1} of Pu [41], and a natural zircon with a U weight concentration around 1 wt% (determined in zircon crystals from the Saranac Prospect, Bancroft, Ontario) [42].

3.1.1. Calculation of the number of detected α-tracks

The theoretical number of α-tracks detected by α-autoradiography techniques, n_α, for a solid sample is given by Eq. (5)

$$n_\alpha = \frac{\pi}{12} \times K \times N_A \times t_{ini} \times \eta_\alpha \times \eta'_\alpha \times \rho_P \times {d_P}^3 \times [\frac{C_U}{M_U} \times (\sum_{i=234,235,238}(X_{iU} \times \lambda_{iU}) + \sum_{j=1}^{n}(X_{Udp,j} \times \lambda_{Udp,j})) + \frac{C_{Pu}}{M_{Pu}} \sum_{i=239,240}(X_{iPu} \times \lambda_{iPu})] \quad (5)$$

Where K is the detector efficiency (ratio of the number of registered α tracks and the theoretical α emitted), N_A is the Avogadro constant, t_{ini} is the integration time processed for experimental analysis (10 days) (s), η_α is the transmission coefficient of α-nuclei within the particle, η'_α transmission coefficient of α-nuclei between the particle and the detector, ρ_P is the particle density (g·cm^{-3}), d_P is the equivalent particle diameter (cm), C_U is the weight concentration of U in the particle (0.88 g·g^{-1} for pure UO_2, ~10^{-3} g·g^{-1} for zircon), C_{Pu} is the weight concentration of Pu in the particle (~0.05 g·g^{-1} for MOX), M_U is the molar mass of U, M_{Pu} is the molar mass of Pu, X_{iU} is the total isotope abundance of ^{234}U, ^{235}U and ^{238}U isotopes in U, X_{iPu} is the total isotope abundance of ^{239}Pu and ^{240}Pu isotopes in Pu, $X_{Udp,j}$ is the abundance of U decay products: $\sum_{j=1}^{n}(X_{Udp,j} \times \lambda_{Udp,j}) = 6 \times X_{^{234}U} \times \lambda_{^{234}U} = 6 \times X_{^{238}U} \times \lambda_{^{238}U}$ in the case of naturally-occurring U at secular equilibrium or negligible if the U had been chemically purified (U from FDNPP), λ is the

disintegration constant of the radionuclides (s^{-1}). According to the literature, the efficiency (K) of IP for α detection is 64% (derived from [27] and [33] based on ^{239}Pu), while it reaches 51% for the BeaQuant® device (derived from [37]).

The determination of the exact value of the product $\eta_\alpha \times \eta'_\alpha$ was not carried out in this work because it is difficult to estimate. It depends on (1) the particle composition which contained the α-emitting radionuclides, (2) the distribution of the α-emitting radionuclides within the particles (i.e. homogeneously distributed or not, as inclusions, etc.), (3) the radionuclide itself (particle type and emission energy) and (4) the collodion layer thickness into which particles are trapped [37]. Three transmission values were assumed for calculation: 0.01, 0.1 and 1, which correspond to low, medium and high transmissions respectively.

3.1.2. Calculation of the fission-tracks (FT) detected number

The theoretical number of FT (n_f) observed in 2π-steradian can also be estimated for the same types of particles according to Eq. (6) modified equation from [43]:

$$n_{FT} = \frac{\pi}{6} \times K_{dry} \times N_A \times t_{ir} \times \eta_{FT} \times \eta'_{FT} \times \rho_P \times d_P^{\,3} \times \phi \times \left(\frac{X_{235_U} \times C_U \times \sigma_{235_U}}{M_U} + \frac{X_{239_{Pu}} \times C_{Pu} \times \sigma_{239_{Pu}}}{M_{Pu}} \right) \quad (6)$$

Where K_{dry} is the track registration efficiency of Lexan®, which is estimated to 96 % ± 4 % [44], N_A is the Avogadro constant, t_{ir} is the irradiation time processed for experimental analysis (s), η_{FT} is the transmission coefficient of fission fragment within the particle , η'_{FT} is the transmission coefficient of fission fragment between the particle and the detector (the product $\eta_{FT} \times \eta'_{FT}$ is determined to be 1), ρ_P is the particle density ($g \cdot cm^{-3}$), d_P is the equivalent particle diameter (cm), ϕ is the thermal neutron flux (1.00×10^{15} neutrons·cm^{-2}) provided by the TRIGA reactor, σ is the

fission cross section under thermal neutrons, (5.80 x 10^{-22} cm² for ^{235}U and 7.42 x 10^{-22} cm² for ^{239}Pu), X_{235U} is the total isotope abundance of ^{235}U in U, X_{239Pu} is the total isotope abundance of ^{239}Pu in Pu, C_U is the weight concentration of U in the particle (0.88 g·g^{-1} for pure UO_2, ~10^{-3} g·g^{-1} for zircon), C_{Pu} is the weight concentration of Pu in the particle (~0.05 g·g^{-1} for MOX), M_U is the molar mass of U, M_{Pu} is the molar mass of Pu.

3.1.3. Comparison of the α-autoradiography and FT methods theoretical performance for the actinide-bearing particles of interest

These calculations are applied on elemental compositions chosen previously. Results are plotted in **Fig. 2**.

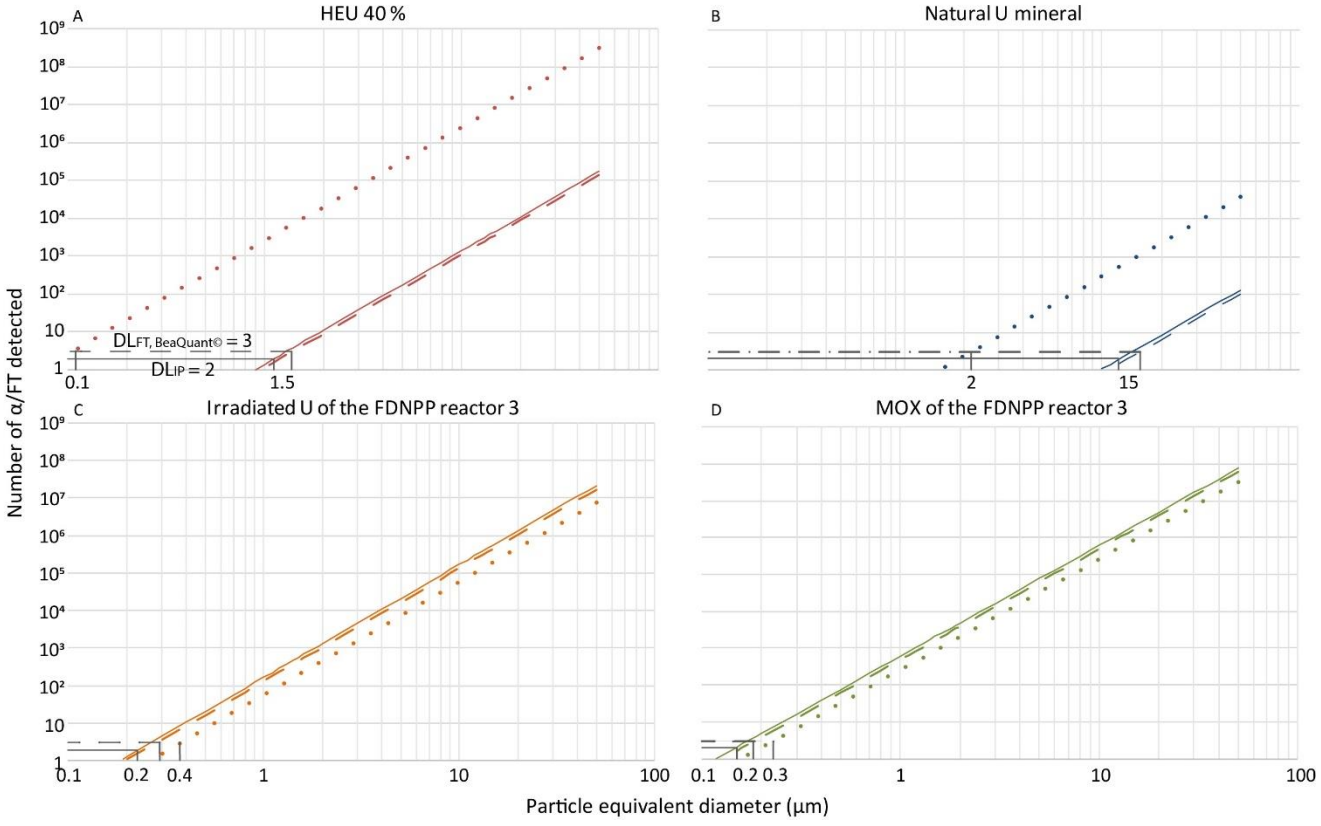

Fig. 2 Graphical representation of theoretical calculation results for $\eta_\alpha \times \eta'_\alpha = 1$ (high transmission) expressed as the number of detected α-tracks/FT plotted against particle size, particle composition

and technique used, with logarithmic scales for both axes. A: HEU 40 %; B: Natural U mineral; C: Irradiated U from the FDNPP reactor 3; D: MOX of the FDNPP reactor 3 (for graphs C and D the burnup average values determined by [41] are considered). Colored solid lines represent results for IP; colored dashed line represent results for BeaQuant®; colored dotted lines represent results for FT. The black lines represent the detection limits of each method in our analytical conditions (see **Table 1**). Results for $\eta_\alpha \times \eta'_\alpha = 0.1$ (medium transmission) and $\eta_\alpha \times \eta'_\alpha = 0.01$ (low transmission) are given in supplementary information B.

The theoretical calculations demonstrate the impact of the transmission coefficient and particle size and composition on detecting of α-emissions. For a transmission coefficient of the α nuclei equal to 1 ($\eta_\alpha \times \eta'_\alpha = 1$), the theoretical calculations show that only HEU particles larger than 1 µm can be detected by IP and the BeaQuant®, whereas HEU particles larger than 0.1 µm can theoretically be detected with the FT method. Regarding the naturally occurring U particles, they can be detected by all of three methods respectively with a full transmission of the α-nuclei for equivalent diameters larger than 15 µm for IP and BeaQuant®, and larger than 2 µm for FT. By contrast, detection of irradiated U particles and reactor 3 MOX particles with equivalent diameters larger than 0.2 µm is possible even with the lowest transmission factor ($\eta_\alpha \times \eta'_\alpha = 0.01$) by means of the three tested methods. Actually, as explained by [45], a small fraction of Pu in U (in the 10^{-3} – 10^{-2} range) strongly increases the number of α-emissions.

Accordingly, the FT method may be the method offering the best chance of detecting U bearing-particles from FDNPP with an equivalent diameter greater than 0.3 µm.

3.2. Experimental results

Results of the comparison of the three localisation methods for particles that create FT or α-track clusters above the detection limits are summarized in **Table 1**. Regarding the BeaQuant®, we gathered the results obtained with the two-acquisition methods (methods 1 and 2), as the same post-processing was implemented for the two methods.

Table 1 Results obtained with the three-localisation methods tested in this study. "/" corresponds to sample not analysed. For IP and BeaQuant® values of background noise and detection limits reported here are the averages for all of our experiments for all samples. Background noise and detection limits for the FT, IP and BeaQuant® methods are expressed in number of fission tracks observed per cluster, number of α-tracks observed per cluster, and counts per pixel, respectively.

Localisation method	Background noise	Detection limit (DL) for a cluster	Number of clusters detected for samples					
			HEU MP 19A32	HEU MP 19A33	Okuma 20B2	Okuma 20B16	Okuma 20B20	Control
FT	1	3	4	4	3	2	1	/
IP	2	6	0	/	9	1	14	/
BeaQuant®	1	3	/	0	0	3	1	1

Background noise is determined for parts of the detector without radioactive particles. The detection limit values are calculated according to the Eq. (7):

$$DL = mean_{background} + 3 \times RSD \quad (7)$$

The FT method allows locating particles that contain fissile nuclei for both HEU MP and Okuma disks (**Fig. 3**). The advantage of this method that it is insensitive to the background associated with the high activity of ^{137}Cs.

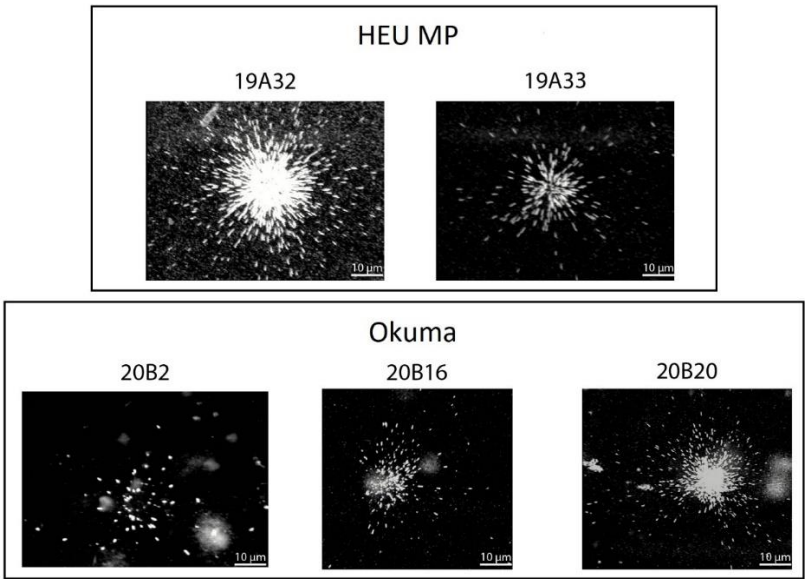

Fig. 3 Images of large FT clusters (more than 30 tracks) observed for HEU MP sample disks and Okuma sample disks. Observations were made with a binocular glass (× 6.5).

The IP method revealed pixel clusters with significant PSL above DL only for Okuma disks (**Fig. 4.c**).

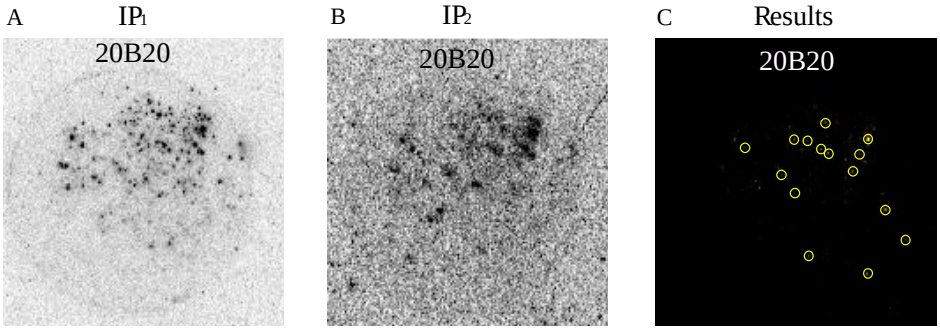

Fig. 4 A: Autoradiography image of IP1 without correction; B: Autoradiography image of IP2 without correction; C: Autoradiography image after processing which allowed localising significant clusters of pixels. Yellow dots correspond to clusters of pixels above DL.

The BeaQuant® has a homogeneous background whatever the sample. Clusters are observed for the Okuma sample (disks 20B16, and 20B20) and for the Control sample (IAEA-472). The detection of one pixel above background for the Control sample, which has a relatively low ^{137}Cs activity (Supplementary information C), suggests that the influence of the β-γ activity is not fully removed. The background observed could be link to radon levels induce by long exposure time and Lexan® disks. However, this method did not allow the detection of α-emitting particles for the HEU MP and for the disk 20B2 of the Okuma.

3.3. Comparison of methods for the localisation of pure U-bearing particles and radioactive particles in a sediment sample from FDNPP

Here we compared the performance of the methods applied to the HEU MP samples that contain only pure micrometric U particles. For these samples, only the FT method allowed the detection of particles as shown in **Table 1**. The inefficiency of IP and BeaQuant® methods may be associated with the particle diameter correlated to the transmission coefficient. As demonstrated in **Fig. 2**, for transmission coefficients respectively equal to 1, 0.1, and 0.01, the equivalent diameter of particles should be higher than 1, 2, and 5 µm to be detected. Accordingly, for detecting pure HEU particles (^{235}U atomic abundance of 40%), only the FT method was efficient. Indeed, SIMS measurements show that most of the HEU particles have diameters between 0.25 to 0.4 µm. This can be explained by (1) the fact that particles are too small (in the micron range) and thus do not contain enough α-emitting nuclei, (2) the transmission coefficient or yield for IP and BeaQuant® methods are too low, or (3) a fading effect may limit their detection by IP [46]. Consequently, α activity could not be detected within 10 days.

The three methods were also applied to the sediment sample Okuma collected near the FDNPP. As explained previously, aliquots of the sample were deposited on three Lexan® disks. The FT method enabled the detection of three particles in the disk 20B2, two particles in the disk 20B16 and one in disk 20B20.

However, the IP method did not allow the detection of α-emitting particles at the same locations on the FT disks, although several clusters of pixels with an intensity higher than the detection limit were detected at other locations (**Fig. 5**). The pixel clusters (set of pixels with a spatial resolution of 150 dpi (169 µm)) can be induced by β-γ emissions of radio-cesium and by radon levels which may impact background levels with long exposure time, that were not fully removed by the data treatment. It cannot be mineral particles that contain naturally occurring U as these particles would also have been detected by means of the FT method.

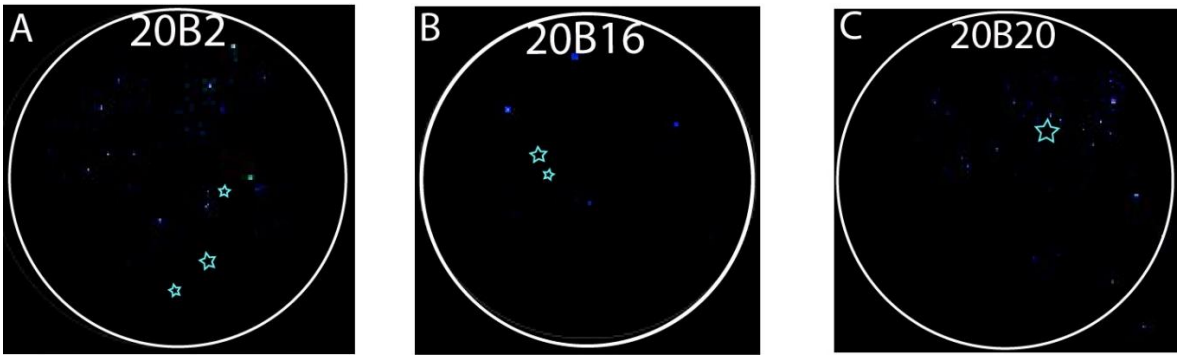

Fig. 5 Comparison between FT and IP results for disks 20B20 (A), 20B16 (B), and 20B2 (C). Star shapes correspond to the location of FT clusters and blue points correspond to clusters of pixels detected by IP (reading with a resolution of 150 dpi (169 µm)).

The BeaQuant® device showed few pixels with values above the DL, i.e. with 3 or 4 counts (pixel resolution: 400 µm). However, again, when results are compared to those of the FT method,

no correlation is observed whereas any types of α-emitter-bearing particles would have been detected with the FT method. So false pixel detection on the Control sample and blank samples may suggest that the BeaQuant® settings and/or data treatment does not fully remove β contributions (**Fig. 6**). Actually, considering the higher ^{137}Cs activity of the Fukushima samples compared to that of Control sample, we cannot exclude the possibility of an increase of the background due to the β emissions of radio-cesium as observed with IP.

To summarise, no correspondence was observed between on one side the pixels above the DL recorded with the BeaQuant and the clusters of α-tracks above DL with the IP method and on the other side the localisation of FT clusters that exceed the DL.

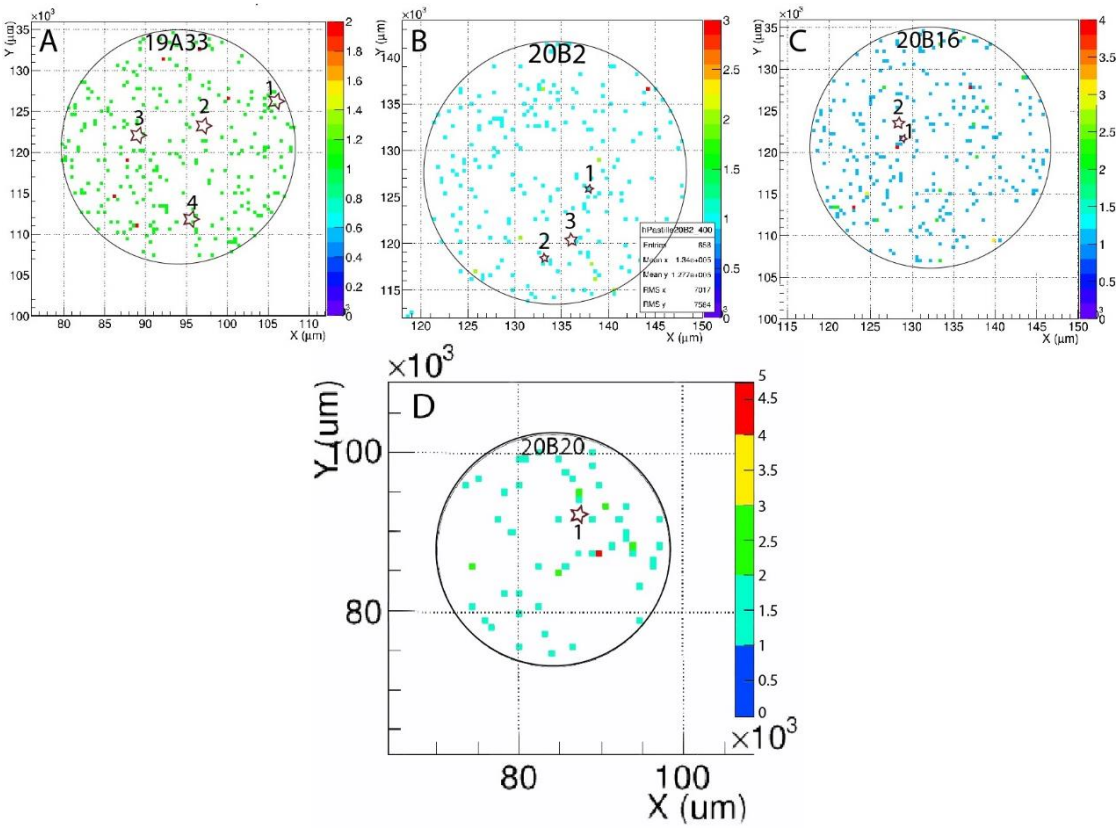

Fig. 6 Comparison between FT and BeaQuant® results (400 × 400 µm²). A: HEU MP sample; B: Okuma disk 20B2; C: Okuma disk 20B16; D: Okuma disk 20B20. Purple star shapes correspond

to the location of FT clusters and coloured pixels correspond to counts detected with the BeaQuant®.

Combination of theoretical calculation and experimental comparison of the three localisation methods revealed that only the FT method allows locating U-bearing particles for the Okuma and HEU MP samples. Several hypotheses can be put forward to explain the absence of particle detection by the two autoradiography methods:

(1) Particles were too small, and consequently α-activities were too low to induce detectable α activity per surface unit (IP pixel size 169 × 169 µm²; BeaQuant® pixel size 400 × 400 µm²).

(2) The layer of organic polymer (collodion) used to fix the sediment particles may significantly reduce the number of α emerging from the surface of the sample disks (low η'_{α}). It should be noted that the collodion thickness is not controlled or known.

(3) The self-absorption phenomenon may be too high if the U is embedded in the form of nanoparticles within larger radioactive microparticles mainly made of silica for instance (low η_{α}). Actually, according to the literature, α-emissions from actinides have a penetration of only a few µm in U-rich minerals [47].

(4) A fading effect may occur for the IP method, which can lead to loss of information for low activities with the two-week long exposure time of this study [46]. Nevertheless, such a long exposure time was mandatory to increase the probability of detecting micrometric particles.

The size and U concentration of the three particles that gave large clusters of FT in disks 20B2, 20B16 and 20B20 were evaluated by SEM-EDS. The particle of the disk 20B2 (**Fig. 7a$_1$**)

438 has a pseudo-spherical shape with a diameter of ~40 µm. The particle on the disk 20B16 (**Fig. 7a$_2$**)
439 has a rod shape with a length of ~50 µm in the longest dimension. The particle on the disk 20B20
440 (**Fig. 7a$_3$**) has no specific shape with a length of ~40 µm. These particles contain elements that are
441 abundant in many minerals including Si, O, Al and Fe (**Fig. 7b$_1$, b$_2$ and b$_3$**) although they also
442 include the following elements: Ti, Mg, Na, K, P and S for disk 20B2, and Zr for disks 20B16 and
443 20B20.
444

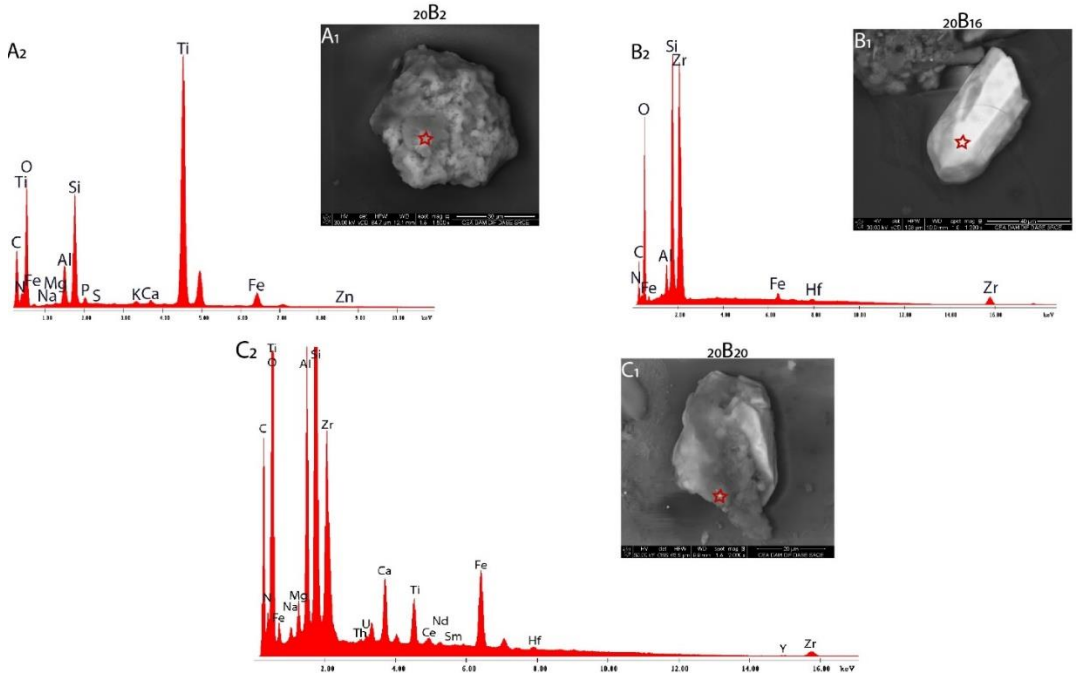

445

446 **Fig. 7** SEM images and EDS spectra of the three particles that produces large clusters (A_1, A_2, B_1,
447 B_2, C_1 and C_2) are presented. A_1: SEM image of the particle of the disk 20B2; A_2: EDS spectrum
448 of the particle of the 20B2 disk; B_1: SEM image of the zircon of disk 20B16; B_2: EDS spectrum
449 of zircon of the disk 20B16; C_1: SEM image of the zircon of the disk 20B20; C_2: EDS spectrum
450 of zircon of the disk 20B20. Red stars represent the spots where EDS spectra were performed.
451

Given their elemental composition and morphology, it is assumed that the particles detected in disks 20B16 and 20B20 are zircons. In contrast, the elemental composition of the particle observed on disk 20B2 is very close to that of the FDNPP-originating particles observed by [4, 10]). However, U was not detected by EDS in the particle found in disk 20B2 despite the observation of a large FT cluster, which may indicate that its concentration remains below the EDS detection limit, i.e. less than 1 wt%.

In the current analytical conditions and in the investigated samples, among the three methods tested, only the FT method allows localising U-bearing particles (natural or anthropogenic). However, as shown by SEM-EDS results on disks 20B16 and 20B2, the FT method itself does not distinguish between natural U particles and those that may originate from FDNPP. Coupling of FT imaging and IP β-γ imaging could allow differentiating between naturally-occurring U in minerals and anthropogenic U-bearing particles from FDNPP. Indeed, the correlation of a FT cluster with an IP pixel cluster of radio-cesium β-γ signals would strongly suggest that the corresponding particle originates from FDNPP. This method was implemented on these three disks. Instead of the IP data treatment described in Eq. 4, the IP1 autoradiography image was treated in order to detect large clusters induced by β-γ emission. The obtained β-γ images were then superimposed with the FT imaging.

In the case of the zircon particles, no correspondence with β signals was found (**Fig. 8B**), whereas in the case of the potential anthropogenic particle a coincidence was clearly observed (**Fig. 8A**). Therefore, this particle has great chances to be anthropogenic, released by FDNPP. Further investigations will be performed on that particle in order to identify its origin. These preliminary results suggest that coupling of FT and β-γ IP can be an alternative technique to determine the source of U-bearing particles. Such result could be improved by coupling FT and

BeaQuant® in β mode thanks to its better pixel resolution and less sensitivity to the ambient background.

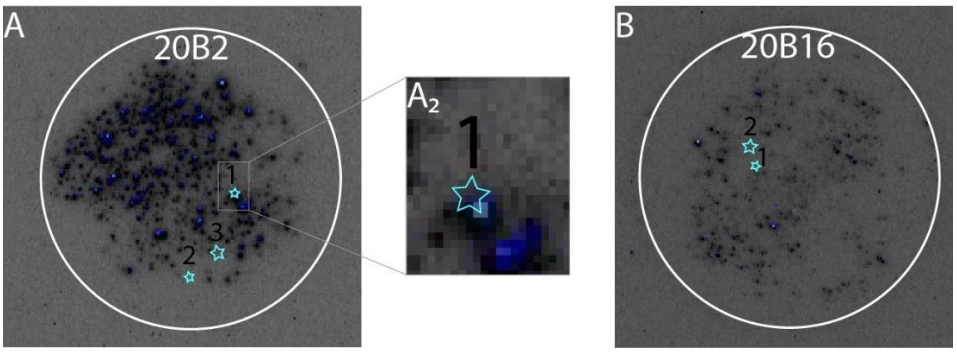

Fig. 8 Superimposition of the localisation FT and β-γ cluster respectively for disks 20B2 and 20B16 (A and B). Light blue stars represent FT clusters.

4. Conclusions

The analytical and experimental results of this study demonstrate that under the chosen analytical conditions and the selected samples the fission track method is more effective than the two tested α-autoradiography methods to detect and localise U-bearing particles.

In this study, HEU MP, as well as particles containing fissile nuclei (natural, or anthropogenic U) in a sediment sample collected in the vicinity of the FDNPP were only recorded by the fission track method. However, the current study also demonstrated that, for a sediment sample, this method alone does not allow to distinguish (1) particles released by FDNPP which contain fragments of nuclear fuel from (2) mineral particles which contain naturally-occurring U. Indeed, our experiments showed that natural zircon minerals with a diameter larger than 10 µm were also detected by means of the FT method. On the contrary, the two α-radiography methods

493 did not provide any results for our samples. This may probably be explained by a too high auto-
494 absorption (1) either in the collodion layer, which is nevertheless required to prevent
495 contamination of the detector by radioactive particles, or (2) possibly within the particles
496 themselves. Nevertheless the results obtained for the two α-radiography methods confirm that
497 presently the developed data treatment did not enable full removal of the contribution of the β
498 and/or γ emitters on the α images. Thus, the implementation of a method coupling the FT efficiency
499 for the detection of α-emitters and the IP efficiency for the detection of β-γ-emitters was tested in
500 order to attempt the discrimination between naturally occurring U-bearing particles and
501 anthropogenic particles. Results are promising because they enabled the distinction between zircon
502 particles and a particle that could potentially come from FDNPP. Restricting the analysis to
503 particles detected by both methods will definitely avoid isolating U-rich minerals and significantly
504 increase the probability of identifying anthropogenic radioactive particles.

505 To conclude, this study opens new perspective for the detection and localisation of U-
506 bearing particles in sediment/soil samples. The combined methodology will be applied to more
507 sediment and soil samples collected in areas located within the main radioactive contamination
508 plume of FDNPP in order to isolate U-bearing particles. The methodology can also probably be
509 improved by coupling the FT method with the BeaQuant® instrument because of its better
510 sensitivity and spatial resolution than IP.

511 ## Acknowledgements

512 Aurélie Diacre received a PhD fellowship from CEA (Commissariat à l'Energie Atomique et aux
513 Energies Alternatives, France). Sample collection was supported by MITATE Lab (CNRS
514 International Research Project) and AMORAD projects (Programme d'Investissements d'Avenir

en Radioprotection et Sûreté Nucléaire, grant no. ANR-11-RSNR-0002). The Ai4R company staff is also acknowledged for the time invested in the current project, including that for optimising acquisitions in α mode and data post-processing. The authors are also grateful to Gabriel Lambrot for formal analysis and Hugues Haedrich for his help to identify the different experimental methods.

References

1. Kashparov VA (2003) Hot Particles at Chernobyl. 10

2. Salbu B, Krekling T, Oughton DH, et al (1994) Hot particles in accidental releases from Chernobyl and Windscale nuclear installations. Analyst 119:125–130. https://doi.org/10.1039/AN9941900125

3. Sandalls FJ, Segal MG, Victorova N (1993) Hot particles from Chernobyl: A review. Journal of Environmental Radioactivity 18:5–22. https://doi.org/10.1016/0265-931X(93)90063-D

4. Abe Y, Iizawa Y, Terada Y, et al (2014) Detection of Uranium and Chemical State Analysis of Individual Radioactive Microparticles Emitted from the Fukushima Nuclear Accident Using Multiple Synchrotron Radiation X-ray Analyses. Anal Chem 86:8521–8525. https://doi.org/10.1021/ac501998d

5. Adachi K, Kajino M, Zaizen Y, Igarashi Y (2013) Emission of spherical cesium-bearing particles from an early stage of the Fukushima nuclear accident. Scientific reports 3:2554. https://doi.org/10.1038/srep02554

6. Imoto J, Ochiai A, Furuki G, et al (2017) Isotopic signature and nano-texture of cesium-rich micro-particles: Release of uranium and fission products from the Fukushima Daiichi Nuclear Power Plant. Scientific Reports 7:5409. https://doi.org/10.1038/s41598-017-05910-z

7. Furuki G, Imoto J, Ochiai A, et al (2017) Caesium-rich micro-particles: A window into the meltdown events at the Fukushima Daiichi Nuclear Power Plant. Scientific Reports 7:1–10. https://doi.org/10.1038/srep42731

8. Kurihara Y, Takahata N, Yokoyama TD, et al (2020) Isotopic ratios of uranium and caesium in spherical radioactive caesium-bearing microparticles derived from the Fukushima Dai-ichi Nuclear Power Plant. Scientific Reports 10:1–10. https://doi.org/10.1038/s41598-020-59933-0

9. Kurihara E, Takehara M, Suetake M, et al (2020) Particulate plutonium released from the Fukushima Daiichi meltdowns. Science of The Total Environment 743:140539. https://doi.org/10.1016/j.scitotenv.2020.140539

10. Martin PG, Griffiths I, Jones CP, et al (2016) In-situ removal and characterisation of uranium-containing particles from sediments surrounding the Fukushima Daiichi Nuclear Power Plant. Spectrochimica Acta Part B: Atomic Spectroscopy 117:1–7. https://doi.org/10.1016/j.sab.2015.12.010

11. Martin PG, Louvel M, Cipiccia S, et al (2019) Provenance of uranium particulate contained within Fukushima Daiichi Nuclear Power Plant Unit 1 ejecta material. Nature Communications 10:1–7. https://doi.org/10.1038/s41467-019-10937-z

12. Martin PG, Jones CP, Cipiccia S, et al (2020) Compositional and structural analysis of Fukushima-derived particulates using high-resolution x-ray imaging and synchrotron characterisation techniques. Scientific Reports 10:1636. https://doi.org/10.1038/s41598-020-58545-y

13. Ochiai A, Imoto J, Suetake M, et al (2018) Uranium Dioxides and Debris Fragments Released to the Environment with Cesium-Rich Microparticles from the Fukushima Daiichi Nuclear Power Plant. Environ Sci Technol 52:2586–2594. https://doi.org/10.1021/acs.est.7b06309

14. Satou Y, Sueki K, Sasa K, et al (2018) Analysis of two forms of radioactive particles emitted during the early stages of the Fukushima Dai-ichi Nuclear Power Station accident. Geochemical Journal 52:137–143. https://doi.org/10.2343/geochemj.2.0514

15. Satou Y, Sueki K, Sasa K, et al (2016) First successful isolation of radioactive particles from soil near the Fukushima Daiichi Nuclear Power Plant. Anthropocene 14:71–76. https://doi.org/10.1016/j.ancene.2016.05.001

16. Igarashi Y, Kogure T, Kurihara Y, et al (2019) A review of Cs-bearing microparticles in the environment emitted by the Fukushima Dai-ichi Nuclear Power Plant accident. Journal of Environmental Radioactivity 205–206:101–118. https://doi.org/10.1016/j.jenvrad.2019.04.011

17. Aarkrog A (1971) Radioecological Investigations of Plutonium in an Arctic Marine Environment. Health Physics 20:31–47

18. Eriksson M, Ljunggren K, Hindorf C (2002) Plutonium hot particle separation techniques using real-time digital image systems. Nuclear Instruments and Methods in Physics Research Section A: Accelerators, Spectrometers, Detectors and Associated Equipment 488:375–380. https://doi.org/10.1016/S0168-9002(02)00438-2

19. Jiménez-Ramos MC, García-López J, García-Tenorio R, García-León M (2009) Characterization of terrestrial hot particles from the Palomares accident using destructive and non-destructive analytical techniques. Radioprotection 44:345–350. https://doi.org/10.1051/radiopro/20095067

20. Jiménez-Ramos MC, García-Tenorio R, Vioque I, et al (2006) Presence of plutonium contamination in soils from Palomares (Spain). Environmental Pollution 142:487–492. https://doi.org/10.1016/j.envpol.2005.10.030

21. Pöllänen R, Ketterer ME, Lehto S, et al (2006) Multi-technique characterization of a nuclearbomb particle from the Palomares accident. Journal of Environmental Radioactivity 90:15–28. https://doi.org/10.1016/j.jenvrad.2006.06.007

22. Donohue DL (2002) Peer Reviewed: Strengthened Nuclear Safeguards. Anal Chem 74:28 A-35 A. https://doi.org/10.1021/ac021909y

23. Jaegler H, Pointurier F, Onda Y, et al (2018) Plutonium isotopic signatures in soils and their variation (2011-2014) in sediment transiting a coastal river in the Fukushima Prefecture, Japan. Environmental Pollution 240:167–176. https://doi.org/10.1016/j.envpol.2018.04.094

24. Esaka KT, Esaka F, Inagawa J, et al (2004) Application of Fission Track Technique for the Analysis of Individual Particles Containing Uranium in Safeguard Swipe Samples. Jpn J Appl Phys 43:L915. https://doi.org/10.1143/JJAP.43.L915

25. Sardini P, Angileri A, Descostes M, et al (2016) Quantitative autoradiography of alpha particle emission in geo-materials using the Beaver™ system. Nuclear Instruments and Methods in Physics Research Section A: Accelerators, Spectrometers, Detectors and Associated Equipment 833:15–22. https://doi.org/10.1016/j.nima.2016.07.003

26. Furuki G, Imoto J, Ochiai A, et al (2017) Caesium-rich micro-particles: A window into the meltdown events at the Fukushima Daiichi Nuclear Power Plant. Scientific Reports 7:1–10. https://doi.org/10.1038/srep42731

27. Haudebourg R, Fichet P (2016) A non-destructive and on-site digital autoradiography-based tool to identify contaminating radionuclide in nuclear wastes and facilities to be dismantled. J Radioanal Nucl Chem 309:551–561. https://doi.org/10.1007/s10967-015-4610-7

28. Chartin C, Evrard O, Onda Y, et al (2013) Tracking the early dispersion of contaminated sediment along rivers draining the Fukushima radioactive pollution plume. Anthropocene 1:23–34. https://doi.org/10.1016/j.ancene.2013.07.001

29. IAEA (2019) Environmental Sample Particle Analysis Interlaboratory Comparison

30. Bonnet T, Comet M, Denis-Petit D, et al (2013) Response functions of imaging plates to photons, electrons and 4He particles. Review of Scientific Instruments 84:103510. https://doi.org/10.1063/1.4826084

31. Chen B, Zhuo W, Kong Y (2011) Identification and counting of alpha tracks by using an imaging plate. Radiation Measurements 46:371–374. https://doi.org/10.1016/j.radmeas.2011.01.002

32. Billon S, Sardini P, Leblond S, et al (2018) MAUD PROJECT-Comparative study of 3 Digital Autoradiography Techniques for characterization: Gas Detector -Solid Scintillation Detector -Phosphor Screens

33. Rahman NM, Iida T, Yamazawa H, Moriizumi J (2006) Determination of Alpha Particle Detection Efficiency of an Imaging Plate (IP) Detector. Jpn J Health Phys 41:272–278. https://doi.org/10.5453/jhps.41.272

34. Fichet P, Bresson F, Leskinen A, et al (2012) Tritium analysis in building dismantling process using digital autoradiography. J Radioanal Nucl Chem 291:869–875. https://doi.org/10.1007/s10967-011-1423-1

35. Radulović V, Kolšek A, Fauré A-L, et al (2018) Qualification of heavy water based irradiation device in the JSI TRIGA reactor for irradiations of FT-TIMS samples for nuclear safeguards. Nuclear Instruments and Methods in Physics Research Section A: Accelerators, Spectrometers, Detectors and Associated Equipment 885:139–144. https://doi.org/10.1016/j.nima.2017.12.046

36. Donnard J, Berny R, Carduner H, et al (2009) The micro-pattern gas detector PIM: A multi-modality solution for novel investigations in functional imaging. Nuclear Instruments and Methods in Physics Research Section A: Accelerators, Spectrometers, Detectors and Associated Equipment 610:158–160. https://doi.org/10.1016/j.nima.2009.05.186

37. Billon S, Sardini P, Angileri A, et al (2020) Quantitative imaging of 226Ra ultratrace distribution using digital autoradiography: Case of doped celestines. Journal of Environmental Radioactivity 217:106211. https://doi.org/10.1016/j.jenvrad.2020.106211

38. Donnard J, Arlicot N, Berny R, et al (2009) Advancements of labelled radio-pharmaceutics imaging with the PIM-MPGD. J Inst 4:P11022–P11022. https://doi.org/10.1088/1748-0221/4/11/P11022

39. Donnard J, Thers D, Servagent N, Luquin L (2009) High Spatial Resolution in β-Imaging With a PIM Device. IEEE Transactions on Nuclear Science 56:197–200. https://doi.org/10.1109/TNS.2008.2005673

40. Angileri A, Sardini P, Beaufort D, et al (2020) Mobility of daughter elements of 238U decay chain during leaching by In Situ Recovery (ISR): New insights from digital autoradiography. Journal of Environmental Radioactivity 220–221:106274. https://doi.org/10.1016/j.jenvrad.2020.106274

41. Nishihara K, Iwamoto H, Suyama K (2012) Estimation of fuel compositions in Fukushima-Daiichi nuclear power plant. 202. https://doi.org/JAEA-Data/Code-2012-018

42. Nasdala L, Hanchar JM, Rhede D, et al (2010) Retention of uranium in complexly altered zircon: An example from Bancroft, Ontario. Chemical Geology 269:290–300. https://doi.org/10.1016/j.chemgeo.2009.10.004

43. Kalsi PC, Sawant PD, Ramaswami A, Manchanda VK (2007) Track etching characteristics of polyester track detector and its application to uranium estimation in seawater samples. J Radioanal Nucl Chem 273:473–477. https://doi.org/10.1007/s10967-007-6845-4

44. Khan HA, Durrani SA (1972) Efficiency calibration of solid state nuclear track detectors. Nuclear Instruments and Methods 98:229–236. https://doi.org/10.1016/0029-554X(72)90103-6

45. Jaegler H, Pointurier F, Onda Y, et al (2019) Method for detecting and characterising actinide-bearing micro-particles in soils and sediment of the Fukushima Prefecture, Japan. J Radioanal Nucl Chem 321:57–69. https://doi.org/10.1007/s10967-019-06575-w

46. Muuri E, Sorokina T, Donnard J, et al (2019) Electronic autoradiography of 133Ba particle emissions; diffusion profiles in granitic rocks. Applied Radiation and Isotopes 149:108–113. https://doi.org/10.1016/j.apradiso.2019.04.026

47. Angileri A, Sardini P, Donnard J, et al (2018) Mapping 238U decay chain equilibrium state in thin sections of geo-materials by digital autoradiography and microprobe analysis. Applied Radiation and Isotopes 140:228–237. https://doi.org/10.1016/j.apradiso.2018.06.018

Supplementary information

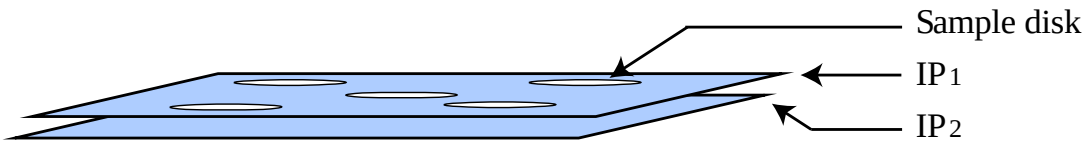

A: Scheme of imaging plate experiments.

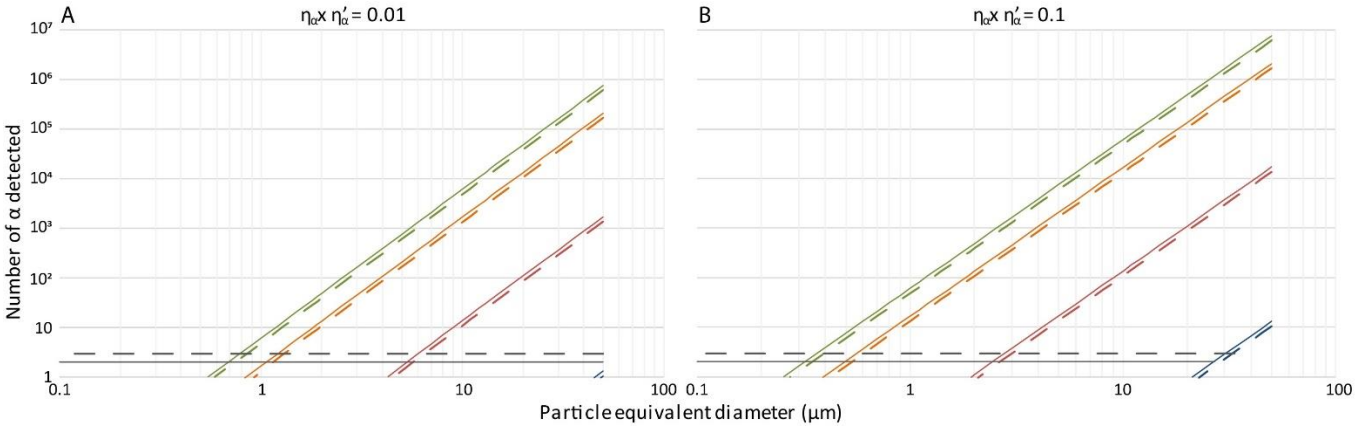

B: Graphical representation of theoretical calculation results for products A. η_α x η'_α = 0.1 (medium transmission) and B. η_α x η'_α = 0.01 (low transmission) expressed as the number of alpha/FT detected as a function of particle size, composition and technique used, at logarithmic scale. Colored solid line represent results for IP, colored dashed line represent results for BeaQuant®. These same black lines represent the detection limits of each method in our analytical conditions. Green line is for MOX of the FDNPP reactor 3; Orange line is for Irradiated U of the FDNPP reactor 3; Pink line is for HEU 40%; Blue line is for Natural U mineral.

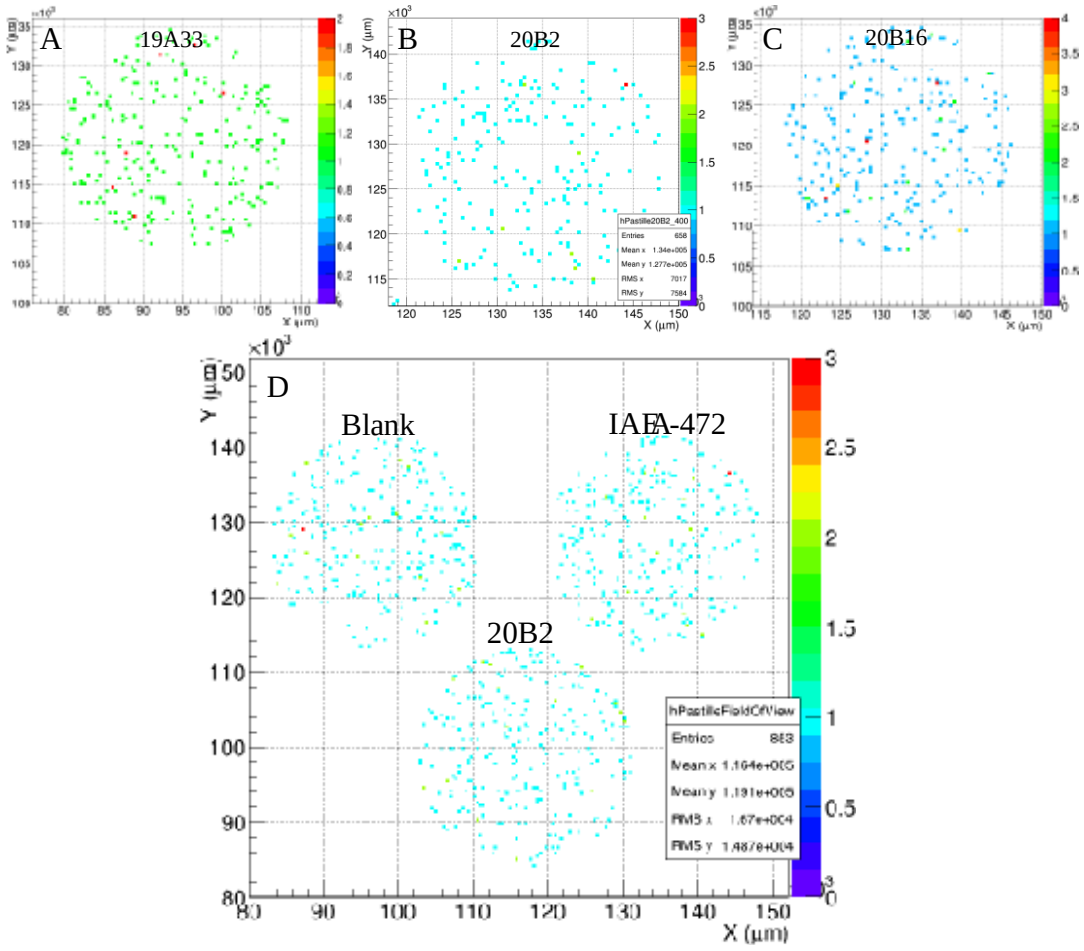

681 **C**: BeaQuant® results after the application of low amplitude filter A. Quality control disk 19A33;

682 Fukushima samples; B. 20B2 (two acquisitions) and C. 20B16; D. Blank and IAEA-472 samples.

683